JPE 16-3-20

http://dx.doi.org/10.6113/JPE.2016.16.3.1025
ISSN(Print): 1598-2092 / ISSN(Online): 2093-4718

Design of a Low-Order Sensorless Controller by Robust H∞ Control for Boost Converters

Xutao Li†, Minjie Chen*, Hirofumi Shinohara*, and Tsutomu Yoshihara*

†,*Graduate School of Information, Production and Systems, Waseda University, Fukuoka, Japan

Abstract

Luenberger observer (LO)-based sensorless multi-loop control of a converter requires an iterative trial-and-error design process, considering that many parameters should be determined, and loop gains are indirectly related to the closed-loop characteristics. Robust H∞ control adopts a compact sensorless controller. The algebraic Riccati equation (ARE)-based and linear matrix inequality (LMI)-based H∞ approaches need an exhaustive procedure, particularly for a low-order controller. Therefore, in this study, a novel robust H∞ synthesis approach is proposed to design a low-order sensorless controller for boost converters, which need not solve any ARE or LMI, and to parameterize the controller by an adjustable parameter behaving like a "knob" on the closed-loop characteristics. Simulation results show the straightforward closed-loop characteristics evaluation and better dynamic performance by the proposed H∞ approach, compared with the LO-based sensorless multi-loop control. Practical experiments on a digital processor confirmed the simulation results.

Key words: Boost converter, Closed-loop characteristics, Low order, Robust H∞ control, Sensorless

I. INTRODUCTION

The controller of a switching converter must guarantee that power conversion is stable under all operating conditions and that the desired dynamic performance is maintained when a disturbance occurs in the input voltage or load. The dynamic performance of a switching converter, whether it has a single-loop or multi-loop control, is determined by its closed-loop characteristics, including audio susceptibility and output impedance [1]. For a single-loop output voltage-controlled buck or boost converter in discontinuous conduction mode, stability and dynamic performance can be guaranteed by making the loop gain as large as possible with high crossover frequency and adequate phase and gain margins because loop gain and crossover frequency are directly related to the closed-loop characteristics. Nevertheless, the transfer function has a right-half-plane zero (RHPZ) from the duty ratio to the output voltage for boost, buck–boost, and flyback converters in continuous conduction mode (CCM) [2]. RHPZ significantly restricts the crossover frequency of the open-loop gain, which results in poor dynamic performance if single-loop voltage control is adopted. Multi-loop control is extensively adopted to improve dynamic performance. However, a current sampling circuit, such as a shunt resistor with an amplifier, a transformer, or an active filter [3], is required to obtain the inductor or switch current, which causes an increase in cost, size, and weight of the circuit. Sensorless multi-loop control solves these problems by estimating the inductor current [4], [5], [6]. The Luenberger observer (LO) [7] is effective in estimating the inductor current for the sensorless control. However, evident drawbacks exist, including many parameters to be determined in the LO-based sensorless multi-loop control. Moreover, the closed-loop characteristics are indirectly related to the loop gains for the multi-loop control [8], [9]. Consequently, an iterative trial-and-error process is needed to design the LO-based sensorless multi-loop control.

Modern control directly handles the inductor current and capacitor voltage in the time domain. However, a state feedback controller with a state observer, as presented in [10], provides no more benefits to the closed-loop characteristics evaluation than the sensorless multi-loop control. Robust H∞ control, which directly considers disturbance attenuation as the target, provides an approach to designing a compact sensorless controller. Two robust H∞ synthesis methods are mainly adopted in previous studies, namely, algebraic Riccati equation

Manuscript received Mar. 10, 2015; accepted Nov. 28, 2015
Recommended for publication by Associate Editor Sangshin Kwak.
†Corresponding Author: leexutao2014@akane.waseda.jp
Tel: +81-93-692-5349, Waseda University
*Graduate School of Information, Production and Systems, Waseda University, Japan

(ARE)-based [11], [12] and linear matrix inequality (LMI)-based methods [13]. However, these methods have several common drawbacks. One drawback is that an exhaustive search procedure is needed to solve the ARE or LMI; in particular, obtaining a solution for the low-order controller is difficult. The second drawback is that the closed-loop evaluation cannot be simplified to demonstrate its advantages over the conventional sensorless multi-loop control. Moreover, no previous study has introduced the design of a sensorless controller, particularly a low-order controller, which has the advantage of less computational volume or simpler circuit, for switching converters by the robust H∞ control. Therefore, in this study, a novel H∞ synthesis approach is proposed to design a low-order sensorless controller for boost converters. This approach need not solve any ARE or LMI, and most importantly, it parameterizes the controller by an adjustable parameter, which behaves like a "knob" on the dynamic performance. Simulations show a straightforward closed-loop characteristics evaluation and better dynamic performance by the proposed H∞ approach, compared with the LO-based sensorless multi-loop control. Practical experiments on a digital processor confirmed the simulation results.

The following definitions are used in this study:

I : ***Unit matrix***

A^{-1} : ***Inverse of matrix A***

A^{T} : ***Transpose of matrix A***

$\mathrm{Im}(A)$: ***Range space of matrix A***

$Ker(A)$: ***Kernel space of matrix A***

$V^{-}(\Sigma)$: ***Weakly unobservable subspace of system Σ***

$S^{-}(\Sigma)$: ***Strongly controllable subspace of system Σ***

II. Problem Formulation

A. Difficult Design of Conventional Sensorless Multi-Loop Control of Boost Converters

The topology-independent block diagram of the conventional sensorless multi-loop control of a switching converter is shown in Fig. 1. The control system consists of an outer loop T_v and an inner loop T_i. The outer loop provides a reference current for the inner current loop. Current $\hat{\imath}_{LO}$ in the inner loop is an estimated inductor current. F_1, F_2, F_3, F_4, F_5, and Z_p are the transfer functions from the input voltage, load current, and duty ratio to the output voltage and inductor current of the power stage; F_m and F_v are the inner and outer compensators; and G_3, G_4, and G_5 are the transfer functions from the input voltage, duty ratio, and output voltage to the estimated inductor current, respectively. The LO expressed in Eq. (1) is effective in estimating the inductor current of a switching converter for the sensorless multi-loop control.

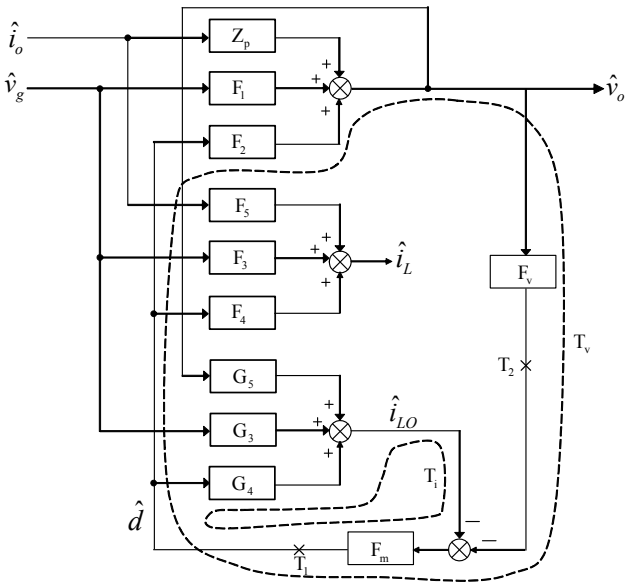

Fig. 1. Small signal block diagram of a sensorless multi-loop control.

$$\begin{bmatrix} \dot{\hat{\imath}}_{LO} \\ \dot{\hat{v}}_{LO} \end{bmatrix} = A \begin{bmatrix} \hat{\imath}_{LO} \\ \hat{v}_{LO} \end{bmatrix} + B \begin{bmatrix} \hat{d} \\ \hat{v}_g \end{bmatrix} + L(\hat{v}_o - \hat{v}_{LO}), \tag{1}$$

where $[\hat{\imath}_{LO}\ \hat{v}_{LO}]$ is the estimated system state and $[\hat{d}\ \hat{v}_g]$ is the system input. Matrices A and B are derived from the small signal model of the converter, whereas L is the parameter of the LO. Transfer functions G_3, G_4, and G_5 can be obtained through Laplace transformation of Eq. (1). From Fig. 1, the closed-loop characteristics, namely, audio susceptibility and output impedance, are written in Eqs. (2) and (3), respectively.

$$\frac{\hat{v}_o(s)}{\hat{v}_g(s)} = \frac{F_1 + F_m(F_1G_4 - F_2G_3)}{1 + F_mG_4 + F_mF_vF_2 + F_mG_5F_2} \tag{2}$$

$$\frac{\hat{v}_o(s)}{\hat{\imath}_o(s)} = \frac{Z_p + F_mZ_pG_4}{1 + F_mG_4 + F_mF_vF_2 + F_mG_5F_2} \tag{3}$$

Transfer functions F_1, F_2, F_3, F_4, F_5, and Z_p are fixed for a given converter. The closed-loop characteristics expressed in Eqs. (2) and (3) are dominated not only by compensators F_m and F_v but also by transfer functions G_3, G_4, and G_5. The design of an LO-based sensorless multi-loop control has the following process: select parameter L of the LO; design compensators F_m and F_v; evaluate closed-loop stability by examining loop gains at points T_1 and T_2 in Fig. 1; evaluate the closed-loop characteristics expressed in Eqs. (2) and (3); and repeat the design process until the desired dynamic performance is maintained. The design process shows the difficulty in designing a conventional sensorless multi-loop control for a converter because of the need to determine many parameters and because the closed-loop characteristics are indirectly related to the loop gains $T_i = F_mG_4$ and $T_v = F_mF_vF_2 + F_mG_5F_2$.

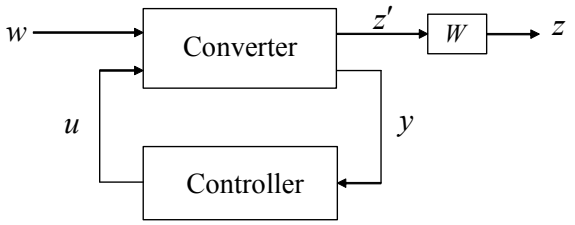

Fig. 2. Block diagram of robust H∞ control.

B. Problems of Previously Proposed Robust H∞ Control for Boost Converters

The block diagram of the robust H∞ control of a switching converter is shown in Fig. 2. The disturbance from the input voltage and load is $w \in R^l$, the controlled output is $z \in R^q$, the controller output is $u \in R^m$, and the measured output is $y \in R^p$. A weight matrix W is used to adjust disturbance attenuation on the controlled output z. The definition for the state space equation of the converter is expressed in Eq. (4). A compact sensorless controller, also called measurement feedback controller, is written in Eq. (5).

$$Converter: \begin{cases} \dot{x} = Ax + Bu + Ew \\ y = C_1 x + D_1 w \\ z = C_2 x + D_2 u \end{cases}, \tag{4}$$

$$Controller: \begin{cases} \dot{p} = Kp + Ly \\ u = Mp + Ny \end{cases}, \tag{5}$$

where $x \in R^n$ is the system state including the inductor current and capacitor voltage.

Generally, the order of the controller in Eq. (5) is the same as that in the system in Eq. (4) with an order n. However, the order of the controller can be reduced to $n - rank[C_1\ D_1] + rank(D_1) \le n$. A low-order controller has the advantage of less computational volume or simpler circuit and is more suitable for real-time control.

Mainly, designing a lower-order controller has two H∞ synthesis approaches. One approach is to solve the AREs as introduced in [14] [15], and the other is to solve the LMIs as introduced in [16] [17]. These synthesis approaches have several common drawbacks. One drawback is that an exhaustive solution search procedure is required to solve the AREs or LMIs. The second drawback is that the closed-loop evaluation cannot be simplified to demonstrate its advantages over the conventional sensorless multi-loop control. Therefore, in this study, a novel H∞ synthesis approach is proposed to design a low-order sensorless controller for boost converters. The proposed H∞ approach need not solve any ARE or LMI, and most importantly, performs a straightforward closed-loop characteristics evaluation by parameterizing the controller with an adjustable parameter that behaves like a "knob" on the dynamic performance.

III. Introduction of the Proposed Robust H∞ Synthesis Approach to the Sensorless Control of Boost Converters

The closed-loop transfer function $G_{cl}(s)$ of the system in Eq. (4) with the controller in Eq. (5), that is, from disturbance w to controlled output z, is written as follows:

$$G_{cl}(s) = C_{cl}(sI - A_{cl})^{-1} B_{cl} + D_{cl}, \tag{6}$$

where:

$$A_{cl} = \begin{bmatrix} A + BNC_1 & BM \\ LC_1 & K \end{bmatrix}, \quad B_{cl} = \begin{bmatrix} E + BND_1 \\ LD_1 \end{bmatrix},$$

$$C_{cl} = \begin{bmatrix} C_2 + D_2 NC_1 & D_2 M \end{bmatrix}, \quad D_{cl} = D_2 ND_1.$$

The main objective of robust H∞ controls is to minimize $G_{cl}(s)$ according to the following H∞ standard:

$$\begin{cases} \|G_{cl}(s)\|_\infty < \gamma \\ Condition: \text{the control object is stabilized} \end{cases}. \tag{7}$$

The basis of the proposed robust H∞ synthesis approach is to decompose the system in Eq. (4) into a special coordinate basis (SCB) [18] [21]. Through SCB decomposition, checking solvability conditions and designing the controller via a step-by-step procedure become easy, as will be presented in the subsequent sections.

A. Solvability Conditions of the Proposed Robust H∞ Synthesis Approach

We denote subsystems $\Sigma_P := (A, B, C_2, D_2)$ and $\Sigma_Q := (A, E, C_1, D_1)$. The solvability conditions of the system in Eq. (4) with the controller in Eq. (5) are as follows:

I) (A, B) is stabilizable;

II) (A, C_1) is detectable;

III) Σ_P and Σ_Q have no invariant zero on the imaginary axis;

IV) $\mathrm{Im}(E) \subset V^-(\Sigma_P) + S^-(\Sigma_P)$;

V) $Ker(C_2) \supset V^-(\Sigma_Q) \cap S^-(\Sigma_Q)$.

I and II are the necessary conditions, whereas III, IV, and V are the sufficient conditions.

B. Design Procedure of a Low-order Controller in Eq. (5)

Referring to [19] [20] [21], the design procedure of a low-order controller in Eq. (5) is as follows:

Step 1: Decompose the system in Eq. (4) into SCB and check the solvability conditions.

Step 2: Compute the H∞ infimum γ^* of the system in Eq. (4).

Step 3: Set any $\gamma > \gamma^*$ and define an auxiliary system in Eq. (8):

$$\begin{cases} \dot{x}_{pq} = A_{pq} x_{pq} + B_{pq} u + E_{pq} w_{pq} \\ y = C_{1p} x_{pq} + D_{1pq} w_{pq} \\ z_{pq} = C_{2p} x_{pq} + D_{2pq} u \end{cases}, \tag{8}$$

where:

$$A_{pq} := A + EE^T P\gamma^{-2} + (\gamma^2 I - QP)^{-1} QC_{2p}^T C_{2p},$$

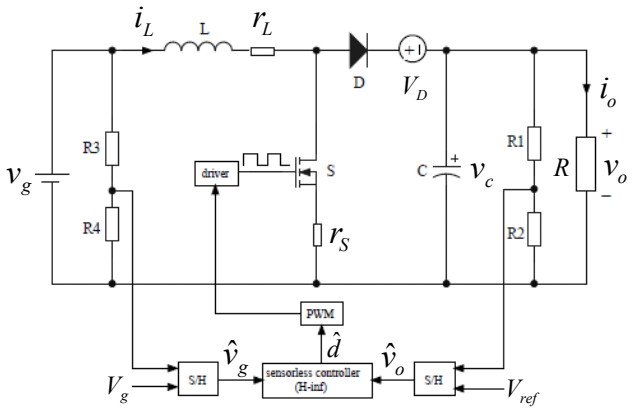

Fig. 3. A sensorless controlled boost converter.

$$B_{pq} := B + (\gamma^2 I - QP)^{-1} Q C_{2p}^T D_{2p},$$

$$E_{pq} := (I - QP\gamma^{-2})^{-1} E_q,$$

$$C_{1p} := C_1 + D_1 E^T P \gamma^{-2}.$$

Through SCB decomposition of Eq. (4), P, Q, C_{1p}, D_{1pq}, C_{2p}, and D_{2pq} can be obtained.

Step 4: Transform the system in Eq. (8) to the following form:

$$\begin{cases} \dot{x} = \begin{bmatrix} A_{11} & A_{12} \\ A_{21} & A_{22} \end{bmatrix} x + \begin{bmatrix} B_1 \\ B_2 \end{bmatrix} u + \begin{bmatrix} E_1 \\ E_2 \end{bmatrix} w_{pq} \\ y = \begin{bmatrix} 0 & C_{1,02} \\ I_k & 0 \end{bmatrix} x + \begin{bmatrix} D_{1,0} \\ 0 \end{bmatrix} w_{pq} \\ z = \begin{bmatrix} C_{2,1} & C_{2,2} \end{bmatrix} x + D_2 u \end{cases}. \quad (9)$$

Step 5: Design a full state feedback controller $u = F_P(\gamma, \varepsilon)x$ for the following subsystem of the system in Eq. (9):

$$\begin{cases} \dot{x} = Ax + Bu + Ew_{pq} \\ y = x \\ z = C_{2p} x + D_{2pq} u \end{cases}. \quad (10)$$

Step 6: Design a full state feedback controller $u = K_Q(\gamma, \varepsilon)x$ for the following subsystem of the system in Eq. (9):

$$\begin{cases} \dot{x} = A_{22}^T x + \begin{bmatrix} C_{1,02}^T & A_{12}^T \end{bmatrix} u + C_{2,2}^T w \\ y = x \\ z = E_2^T x + \begin{bmatrix} D_{1,0}^T & E_1^T \end{bmatrix} u \end{cases}. \quad (11)$$

Step 7: Denote $F_P(\gamma, \varepsilon) = [F_{P1}\ F_{P2}]$ and $K_Q(\gamma, \varepsilon) = [K_{Q1}\ K_{Q2}]$. A low-order controller in Eq. (5) is expressed as follows:

$$\begin{cases} \dot{p} = Kp + Ly \\ u = Mp + Ny \end{cases}, \quad (12)$$

where:

$$K = A_{22} + K_{Q1} C_{1,02} + K_{Q2} A_{12} + (B_2 - K_{Q2} B_1) F_{P2},$$

$$L = \begin{bmatrix} -K_{Q1} & A_{21} + K_{Q2} A_{11} - (A_{22} + K_{Q1} C_{1,02} + K_{Q2} A_{12}) K_{Q2} \end{bmatrix} + (B_2 + K_{Q2} B_1) \begin{bmatrix} 0 & F_{P1} - F_{P2} K_{Q2} \end{bmatrix},$$

$$M = F_{P2},$$

$$N = \begin{bmatrix} 0 & F_{P1} - F_{P2} K_{Q2} \end{bmatrix}.$$

Symbol γ represents the desired disturbance attenuation level satisfying $\gamma > \gamma^*$. γ^* is the H∞ infimum of the system in Eq. (4) and can be computed as introduced in [22] [23]. Parameter $\varepsilon > 0$ is tunable. $\varepsilon^* > 0$ exists, such that, for all $0 < \varepsilon < \varepsilon^*$, the closed-loop system becomes internally stable and γ-suboptimal $\|G_{cl}(s)\|_\infty < \gamma$ is satisfied.

IV. Derivation of a Low-Order Sensorless Controller from the Proposed Robust H∞ Synthesis Approach for Boost Converters

A. Construction of the AC Small Signal Average Value Model of Boost Converters

Fig. 3 shows the boost converter used in this study, in which several parasitic components are considered. Referring to [24], the AC average value model of the boost converter in CCM is written in Eq. (13):

$$\dot{\hat{x}} = A\hat{x} + B\hat{d} + E\hat{w}, \quad (13)$$

where $\hat{x} = [\hat{i}_L\ \hat{v}_c]^T$, $\hat{w} = [\hat{v}_g\ \hat{i}_o]^T$, and

$$A = \begin{bmatrix} -\dfrac{r_L + Dr_s}{L} & -\dfrac{D'}{L} \\ \dfrac{D'}{C} & -\dfrac{1}{RC} \end{bmatrix},\quad B = \begin{bmatrix} \dfrac{(D'R - r_s)V_g + (r_s + r_L)V_D}{L(r_L + Dr_s + D'^2 R)} \\ -\dfrac{V_g - D'V_D}{C(r_L + Dr_s + D'^2 R)} \end{bmatrix},$$

$$E = \begin{bmatrix} \dfrac{1}{L} & 0 \\ 0 & -\dfrac{1}{C} \end{bmatrix},$$

and

$$D' = \frac{r_s V_{ref} + RV_g}{2R(V_{ref} + V_D)} \left(1 + \sqrt{1 - \frac{4R(r_L + r_s)(V_{ref} + V_D)V_{ref}}{(r_s V_{ref} + RV_g)^2}}\right). \quad (14)$$

Symbol D denotes the duty ratio at a given operating point and $D' = 1 - D$, and $\hat{d}$ represents the duty ratio adjustment from the given operating point when a disturbance occurs. Ignoring the equivalent series resistor of the output capacitor, $\hat{v}_c$ is equivalent to $\hat{v}_o$. Here, $\hat{v}_o$ and $\hat{v}_g$ are not scaled by the corresponding dividing resistors in Fig. 3 for the convenience of evaluating the practical closed-loop characteristics. The coefficients of a controller will be scaled at the execution stage on a digital processor.

B. Construction of the State Space Equation for the Proposed Robust H∞ Control

From the AC small signal model in Eq. (13), the state space equation for the proposed robust H∞ control is written as follows:

$$\begin{cases} \dot{\hat{x}} = A\hat{x} + B\hat{d} + E\hat{w} \\ y = C_1\hat{x} + D_1\hat{w} \\ z = C_2\hat{x} + D_2\hat{d} \end{cases} . \quad (15)$$

The matrices A, B, and E are the same as that in Eq. (13), and

$$C_1 = \begin{bmatrix} 0 & 0 \\ 0 & 1 \end{bmatrix}, \ D_1 = \begin{bmatrix} 1 & 0 \\ 0 & 0 \end{bmatrix},$$

$$C_2 = \begin{bmatrix} 1 & 0 \\ 0 & w_o \end{bmatrix}, \ D_2 = \begin{bmatrix} 0 \\ 0 \end{bmatrix}.$$

The measurable output is $y = [\hat{v}_g \ \hat{v}_o]^T$, the controlled output is $z = [\hat{i}_L \ \hat{v}_o]^T$, and w_o is the weight on the output voltage, as shown in Fig. 2. Then, we denote:

$$A = \begin{bmatrix} a_{11} & a_{12} \\ a_{21} & a_{22} \end{bmatrix}, \ B = \begin{bmatrix} b_1 \\ b_2 \end{bmatrix}, \ E = \begin{bmatrix} e_1 & 0 \\ 0 & e_2 \end{bmatrix}.$$

C. SCB Decomposition of the System in Eq. (15)

The SCB decomposition of subsystem $\Sigma_P := (A, B, C_2, D_2)$ can be obtained as follows:

$$\begin{bmatrix} \dot{x}_b \\ \dot{x}_d \end{bmatrix} = \begin{bmatrix} a_{22} - \frac{b_2 a_{12}}{b_1} & w_o(a_{21} - \frac{b_2(a_{11}-a_{22})}{b_1} - \frac{b_2^2 a_{12}}{b_1^2}) \\ a_{11} + \frac{b_2 a_{12}}{b_1} & \frac{a_{12}}{w_o} \end{bmatrix} \begin{bmatrix} x_b \\ x_d \end{bmatrix} + \begin{bmatrix} 0 \\ b_1 \end{bmatrix} \hat{d} \quad (16)$$

$$\begin{bmatrix} y_d \\ y_b \end{bmatrix} = \begin{bmatrix} x_d \\ x_b \end{bmatrix}$$

and

$$\Gamma_{sP} = \begin{bmatrix} 0 & 1 \\ \frac{1}{w_o} & \frac{b_2}{b_1} \end{bmatrix}, \ \Gamma_{oP} = \begin{bmatrix} 1 & 0 \\ \frac{w_o b_2}{b_1} & 1 \end{bmatrix}, \ \Gamma_{iP} = \frac{1}{b_1}.$$

The SCB decomposition of subsystem $\Sigma_Q := (A^T, C_1^T, E^T, D_1^T)$ can be obtained as follows:

$$\begin{bmatrix} \dot{x}_a^- \\ \dot{x}_d \end{bmatrix} = \begin{bmatrix} a_{11} & a_{21} \\ a_{12} & a_{22} \end{bmatrix} \begin{bmatrix} x_a^- \\ x_d \end{bmatrix} + \begin{bmatrix} 0 & 0 \\ 0 & 1 \end{bmatrix} \begin{bmatrix} u_0 \\ u_d \end{bmatrix}$$

$$\begin{bmatrix} y_0 \\ y_d \end{bmatrix} = \begin{bmatrix} e_1 & 0 \\ 0 & 1 \end{bmatrix} \begin{bmatrix} x_a^- \\ x_d \end{bmatrix} + \begin{bmatrix} 1 & 0 \\ 0 & 0 \end{bmatrix} \begin{bmatrix} u_0 \\ u_d \end{bmatrix} \quad (17)$$

and

$$\Gamma_{sQ} = \begin{bmatrix} 1 & 0 \\ 0 & 1 \end{bmatrix}, \ \Gamma_{oQ} = \begin{bmatrix} 1 & 0 \\ 0 & e_2 \end{bmatrix}, \ \Gamma_{iQ} = \begin{bmatrix} 1 & 0 \\ 0 & 1 \end{bmatrix}.$$

D. Solvability Verification

Proving that solvability conditions I, II, and III in subsection III.A are satisfied is easy. The following expressions can be obtained after SCB decomposition:

$$\mathcal{V}^-(\Sigma_Q) = \mathrm{Im}\{\begin{bmatrix} 1 \\ 0 \end{bmatrix}\}, \ \mathcal{S}^-(\Sigma_Q) = \mathrm{Im}\{\begin{bmatrix} 0 \\ 1 \end{bmatrix}\}.$$

Evidently, $Ker(C_2) \subset R^2$; thus, solvability condition V is also satisfied. Although the SCB decomposition of subsystem Σ_P shows a state x_b, condition IV is unsatisfied, which does not mean that the controller in Eq. (5) for the system in Eq. (15) is unsolvable. It is still solvable; however, a complicated computation of the H∞ infimum γ^* is required, as will be presented in the subsequent sections.

E. Computation of the H∞ Infimum of the System in Eq. (15)

Through SCB decomposition, the H∞ infimum of subsystem Σ_Q is $\gamma_Q^* = 0$. Thus, the H∞ infimum of the system in Eq. (15) is determined only by subsystem Σ_P. Referring to [23], for a given $\gamma > 0$, a positive real symmetric solution s_x to the ARE in Eq. (18) should exist.

$$s_x A_x + A_x^T s_x + s_x E_x E_x^T s_x \gamma^{-2} - s_x B_x B_x^T s_x + C_x^T C_x = 0, \quad (18)$$

where:

$$A_x = a_{22} - \frac{b_2}{b_1} a_{12} - \frac{w_o^2 b_1 b_2}{b_1^2 + w_o^2 b_2^2}(a_{21} - \frac{b_2}{b_1}(a_{11} - a_{22}) - \frac{b_2^2}{b_1^2} a_{12}),$$

$$B_x B_x^T = \frac{w_o^2 b_1^2}{b_1^2 + w_o^2 b_2^2}(a_{21} - \frac{b_2}{b_1}(a_{11} - a_{22}) - \frac{b_2^2}{b_1^2} a_{12})^2,$$

$$C_x^T C_x = \frac{b_1^2}{b_1^2 + w_o^2 b_2^2},$$

$$E_x E_x^T = w_o^2 (\frac{e_1^2 b_2^2}{b_1^2} + e_2^2).$$

According to the existing condition of the previously presented solution, the H∞ infimum of Eq. (15) can be obtained as follows:

$$\gamma^* = \frac{\sqrt{(b_1^2 e_2^2 + b_2^2 e_1^2)(b_1^2 + w_o^2 b_2^2)}}{b_1^2 a_{21} - b_1 b_2 (a_{11} - a_{22}) - b_2^2 a_{12}}. \quad (19)$$

F. Derivation of a Low-order Controller in Eq. (5)

Although the system in Eq. (9) can be constructed through SCB decomposition of the system in Eq. (15), the system in Eq. (15) is already similar to the system in Eq. (9). Therefore, a transformation $T_x = [0\ 1;\ 1\ 0]$ on system state x is performed to transform Eq. (15) into the form in Eq. (9). Following the design procedure described in subsection III.B, a low-order controller in Eq. (5) can be obtained as follows:

$$\begin{cases} \dot{p} = Kp + Ly \\ \hat{d} = Mp + Ny \end{cases}, \quad (20)$$

where:

$$K = -\frac{w_o^2 b_2 (b_1^2 a_{21} - b_1 b_2 (a_{11} - a_{22}) - b_2^2 a_{12}) s_x - b_1^3}{b_1 (b_1^2 + w_o^2 b_2^2)} \frac{\lambda}{\varepsilon},$$

$$L = \begin{bmatrix} e_1 & \frac{w_o^2 (b_1^2 a_{21} - b_1 b_2 (a_{11} - a_{22}) - b_2^2 a_{12}) s_x + w_o^2 b_1 b_2}{b_1^2 + w_o^2 b_2^2} \frac{\lambda}{\varepsilon} \end{bmatrix},$$

$$M = -\frac{a_{11}}{b_1} - \frac{w_o^2 b_2 (b_1^2 a_{21} - b_1 b_2 (a_{11} - a_{22}) - b_2^2 a_{12}) s_x - b_1^3}{b_1^2 (b_1^2 + w_o^2 b_2^2)} \frac{\lambda}{\varepsilon},$$

$$N = \begin{bmatrix} 0 & \frac{w_o^2}{b_1} \frac{(b_1^2 a_{21} - b_1 b_2 (a_{11} - a_{22}) - b_2^2 a_{12}) s_x + b_1 b_2}{b_1^2 + w_o^2 b_2^2} \frac{\lambda}{\varepsilon} - \frac{a_{12}}{b_1} \end{bmatrix}.$$

λ in Eq. (20) can be set to any negative value, for example, −1. Parameter $\varepsilon > 0$ is tunable.

TABLE I
PARAMETERS OF A BOOST CONVERTER

Input voltage	v_g = 10 V
Output voltage	v_o = 20 V
Capacitor	C = 1,000 μF
Inductor	L = 47 μH, r_L = 24 mΩ
Load	R = 25 Ω
Switch	r_S = 36 mΩ
Diode	V_D = 1.25 V
Switching frequency	f_s = 150 kHz

V. SIMULATIONS AND EXPERIMENTS

In this study, a boost converter, with parameters listed in Table I, is used to show the straightforward closed-loop characteristics evaluation by the proposed robust H∞ synthesis approach, compared with the conventional LO-based sensorless multi-loop control.

A. Simulations of the Sensorless Controller Derived from the Proposed H∞ Synthesis Approach

By substituting the parameters in Table 1 into the system in Eq. (13), the following matrices are obtained:

$$A=\begin{bmatrix}-918.8 & -9938.5\\ 467.1 & -40\end{bmatrix},\quad B=\begin{bmatrix}450820\\ -1712.7\end{bmatrix},$$

$$E=\begin{bmatrix}21277 & 0\\ 0 & -1000\end{bmatrix}.$$

By setting $\lambda = -1$, the low-order sensorless controller for the boost converter in Table 1 is obtained in Eq. (21).

First, we set w_o = 1 to examine the closed-loop characteristics. From Eq. (19), the H∞ infimum of the system in Eq. (15) is $\gamma^* = 2.1341$. We set $\gamma = 2.2$; then, $s_x = 0.0053$ can be obtained from Eq. (18). Figs. 4(a) and 4(b) show the closed-loop audio susceptibility and output impedance, respectively, by substituting γ and s_x into Eq. (21). Lower than approximately ε = 1/6,000, the disturbance on the output voltage begins to be attenuated. The disturbance attenuation increases as long as ε decreases. Lower than ε = 1/100,000, disturbance attenuation will clearly not change, particularly for output impedance.

Second, we set w_o = 5 to augment the effect of disturbance attenuation on the output voltage. Similarly, the H∞ infimum of the system in Eq. (15) is $\gamma^* = 2.1628$. We set $\gamma = 2.2$; then, s_x = 0.0022 is obtained. The closed-loop characteristics are shown in Fig. 5. Lower than approximately ε = 1/3,000, the disturbance on the output voltage begins to be significantly

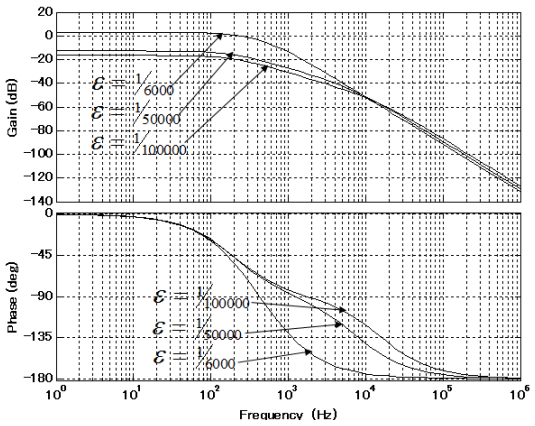

(a) Audio susceptibility.

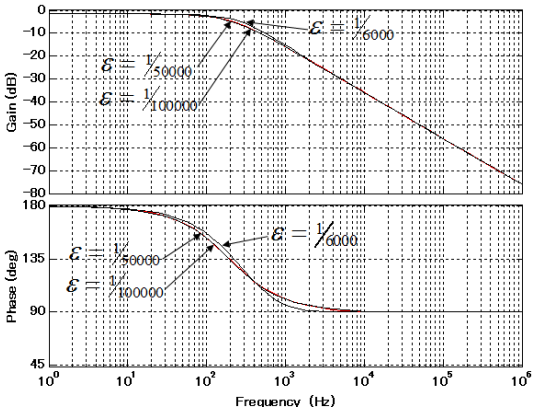

(b) Output impedance.

Fig. 4. Bode plots of closed-loop characteristics (w_o = 1).

attenuated. Lower than ε = 1/20,000, disturbance attenuation will evidently be unchanged.

Then, we set w_o = 10 to further augment the effect of disturbance attenuation on the output voltage. The H∞ infimum of the system in Eq. (15) is $\gamma^* = 2.1640$. We set γ = 2.2; then, s_x = 0.0013 is obtained. The closed-loop characteristics are shown in Fig. 6. Lower than approximately ε = 1/2,000, the disturbance on the output voltage begins to be significantly attenuated. Lower than ε = 1/8,000, disturbance attenuation will evidently be unchanged, which means that the closed-loop characteristics have reached its limit with w_o = 10; thus, this value can be selected as the suitable value for ε.

Although a greater wo value can further enhance the disturbance attenuation on the output voltage, has been obtained. The closed-loop dynamic responses of the output voltage to a step change in the disturbance are shown in Fig. 7 for wo = 10.

For the sensorless controller in Eq. (21), p is equivalent to the estimated inductor current. Through Laplace

$$\begin{cases}\dot{p}=-\dfrac{1.6148\times10^5 w_o^2 s_x+9.1622\times10^4}{9.1622\times10^4+1.3223w_o^2}\dfrac{1}{\varepsilon}p+\begin{bmatrix}2.1277\times10^4 & -\dfrac{9.4283\times10^7 w_o^2 s_x-772.10w_o^2}{2.0323\times10^5+2.9332w_o^2}\dfrac{1}{\varepsilon}\end{bmatrix}\begin{bmatrix}\hat{v}_g\\ \hat{v}_o\end{bmatrix}\\ \hat{d}=(0.0020-\dfrac{1.6148w_o^2 s_x+0.9162}{4.1304\times10^5+5.9613w_o^2}\dfrac{1}{\varepsilon})p+\begin{bmatrix}0 & 0.0220-\dfrac{9.4283\times10^5 w_o^2 s_x-7.7210w_o^2}{9.1622\times10^8+1.3223\times10^4 w_o^2}\dfrac{1}{\varepsilon}\end{bmatrix}\begin{bmatrix}\hat{v}_g\\ \hat{v}_o\end{bmatrix}\end{cases} \quad (21)$$

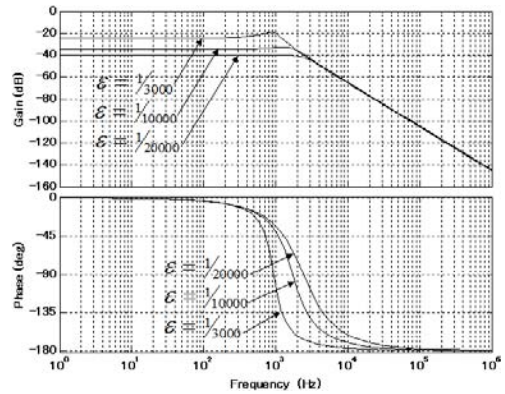

(a) Audio susceptibility

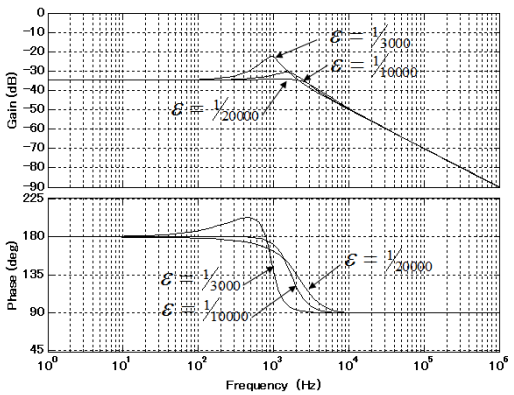

(b) Output impedance

Fig. 5. Bode plots of closed-loop characteristics ($w_o = 5$).

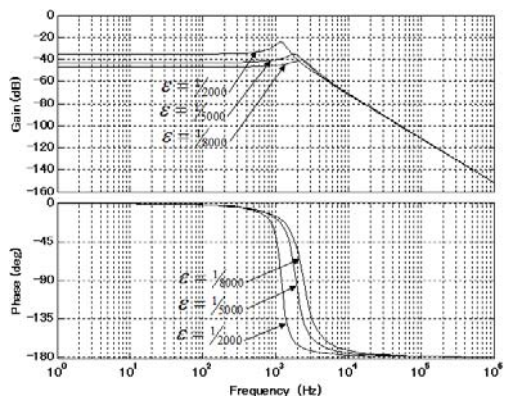

(a) Audio susceptibility

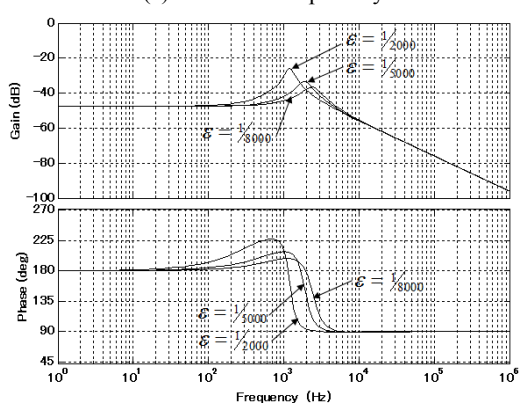

(b) Output impedance

Fig. 6. Bode plots of closed-loop characteristics ($w_o = 10$).

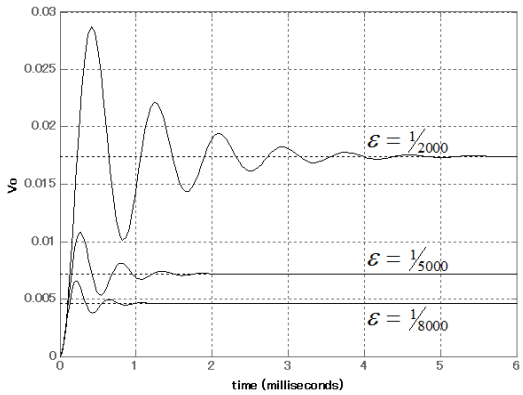

(a) Step response of $\hat{v}_o$ to a step change in $\hat{v}_g$

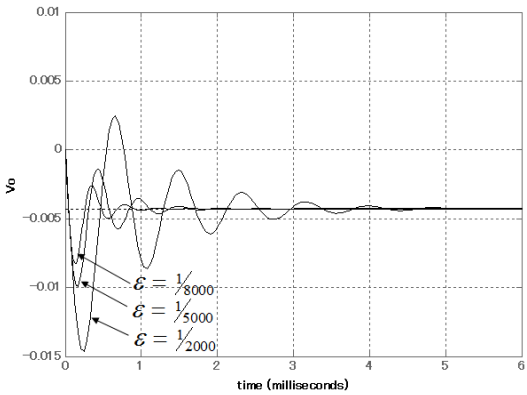

(b) Step response of $\hat{v}_o$ to a step change in $\hat{\imath}_o$

Fig. 7. Step responses of $\hat{v}_o$.

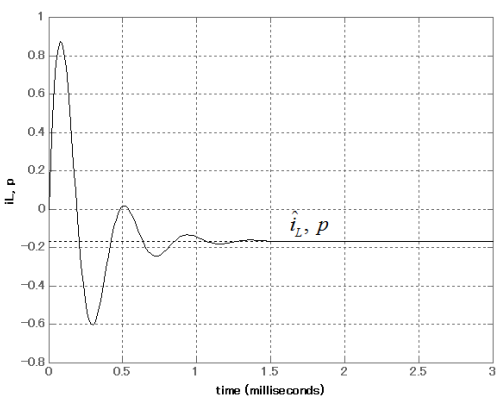

(a) Step responses of $\hat{\imath}_L$ and p to a step change in $\hat{v}_g$

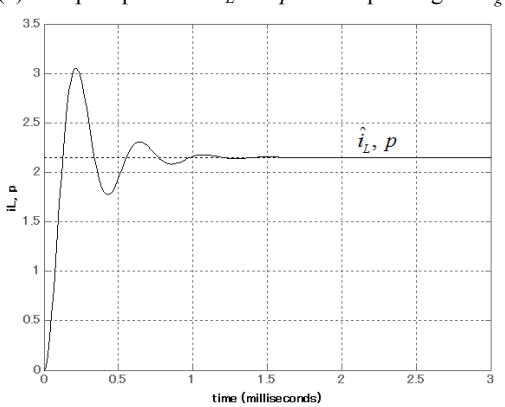

(b) Step responses of $\hat{\imath}_L$ and p to a step change in $\hat{\imath}_o$

Fig. 8. Step responses of $\hat{\imath}_L$ and p.

transformation of Eqs. (21) and (15), transfer functions $p(s)/\hat{v}_g(s)$ and $p(s)/\hat{i}_o(s)$ are obtained. After the parameters listed in Table 1 are substituted, $\hat{i}_L(s)/\hat{v}_g(s) = p(s)/\hat{v}_g(s)$ and $\hat{i}_L(s)/\hat{i}_o(s) = p(s)/\hat{i}_o(s)$ are derived. For $w_o = 10$ and $\varepsilon = 1/8{,}000$, the step responses of $\hat{i}_L$ and p are the same (Fig. 8), which means that p is a complete estimation of the inductor current $\hat{i}_L$.

B. Simulations of the Conventional LO-based Sensorless Multi-loop Control

We denote the current loop $T_i = F_m G_4$ and the voltage loop $T_v = F_m F_v F_2 + F_m G_5 F_2$ in Fig. 1. The overall loop gain at point T_1 is written as $T_1 = T_i + T_v$, and the outer loop gain at point T_2 is written as $T_2 = T_v/1 + T_i$. From the expressions of T_1 and T_2, the crossover frequency of current loop T_i should be as high as possible to provide a 90° phase boost for voltage loop T_v, whereas its gain should be as small as possible at low frequencies. Loop gain T_v should be as large as possible to attenuate the disturbance on the output voltage.

For the boost converter with parameters listed in Table 1, the LO in Eq. (1) is written as follows:

$$\dot{\hat{x}} = \begin{bmatrix} -918.8 & -9{,}938.5 \\ 467 & -40 \end{bmatrix} \hat{x} + \begin{bmatrix} 450{,}820 & 21{,}277 \\ -1{,}712.7 & 0 \end{bmatrix} u + \begin{bmatrix} l_1 \\ l_2 \end{bmatrix} \Delta\hat{v}_o \quad (22)$$

where $\hat{x} = [\hat{i}_{LO}\ \hat{v}_{LO}]$, $u = [\hat{d}\ \hat{v}_g]$, and $\Delta\hat{v}_o = \hat{v}_o - \hat{v}_{LO}$. The PI controllers in Eq. (23) are used as compensators F_m and F_v:

$$F_m = K_{P1} + K_{I1}\frac{1}{s}, \quad F_v = K_{P2} + K_{I2}\frac{1}{s}. \quad (23)$$

In Eqs. (22) and (23), the parameters to be determined are $L = [l_1\ l_2]^T$, K_{P1}, K_{I1}, K_{P2}, and K_{I2}. An iterative trial-and-error design process involves assigning the eigenvalues of $A - LC$ to determine $L = [l_1\ l_2]^T$, where $C = [0\ 1]$; tuning K_{P1}, K_{I1}, K_{P2}, and K_{I2} by examining the bode plots of loop gains $T_1 = T_i + T_v$ and $T_2 = T_v/1 + T_i$ until a stable control system is maintained; further tuning K_{P1}, K_{I1}, K_{P2}, and K_{I2} by examining the closed-loop characteristics in Eqs. (2) and (3) to obtain good dynamic performance; and repeating these steps until the desired dynamic performance is obtained. Through this iterative process, the best eigenvalues $\{-0.0093, -7.5003\} \times 10^5$ are determined, and correspondingly, $L = [0.01\ 0.75]^T \times 10^6$. After the LO is determined, compensators F_m and F_v are used to show the design of compensators F_m and F_v:

$$\begin{aligned} &\text{I.} \quad F_m = 0.20 + 250/s, \ F_v = 30.0 + 18{,}000/s \\ &\text{II.} \quad F_m = 0.40 + 500/s, \ F_v = 30.0 + 18{,}000/s \\ &\text{III.} \quad F_m = 0.20 + 250/s, \ F_v = 45.0 + 25{,}000/s \end{aligned} \quad (24)$$

The bode plots of loop gains T_1 and T_2 are shown in Fig. 9, with the stability characteristics given in Eq. (25).

$$\begin{aligned} &\text{I.} \quad T_1: f_c = 12.9\ \text{kHz}, PM = 78.8° \\ &\qquad T_2: f_c = 2.26\ \text{kHz}, PM = 73.5°, GM = 18.8\ \text{dB} \\ &\text{II.} \quad T_1: f_c = 25.6\ \text{kHz}, PM = 84.3° \\ &\qquad T_2: f_c = 2.28\ \text{kHz}, PM = 77.9°, GM = 18.8\ \text{dB} \\ &\text{III.} \quad T_1: f_c = 12.5\ \text{kHz}, PM = 72.0° \\ &\qquad T_2: f_c = 3.33\ \text{kHz}, PM = 66.4°, GM = 15.3\ \text{dB} \end{aligned} \quad (25)$$

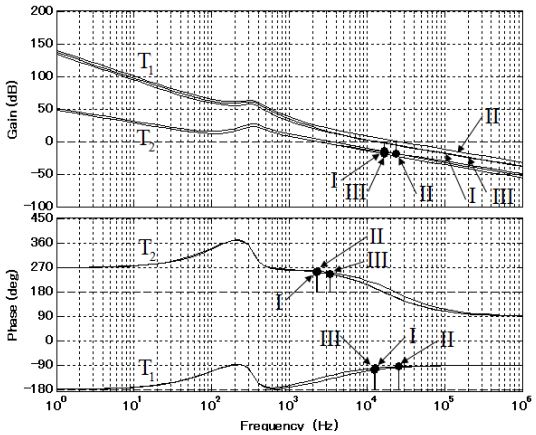

Fig. 9. Bode plots of T_1 and T_2.

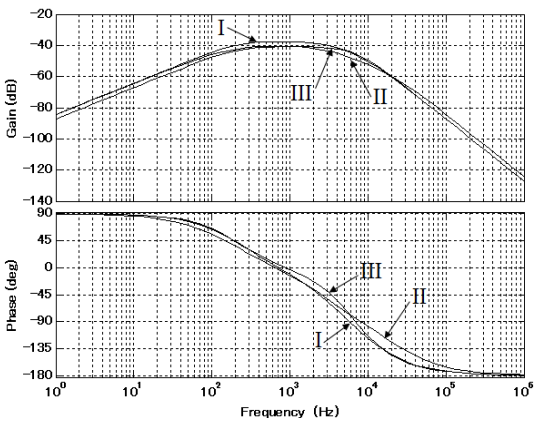

(a) Audio susceptibility.

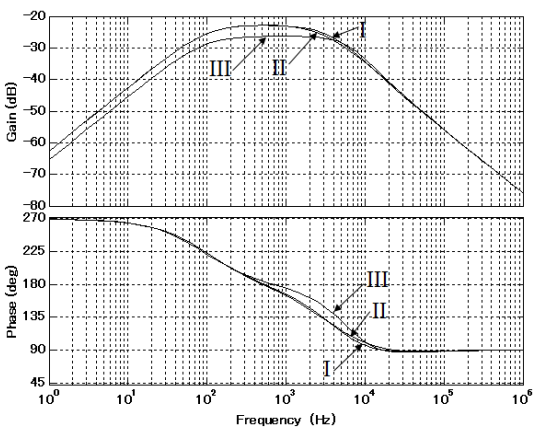

(b) Output impedance.

Fig. 10. Bode plots of closed-loop characteristics.

Fig. 10 shows the closed-loop characteristics in Eqs. (2) and (3), and Fig. 11 shows the step responses of the output voltage. From curves I and II in Figs. 9, 10, and 11, increasing the gain of inner compensator F_m can increase gain crossover frequency and decrease peak output voltage; however, recovery time is prolonged. Curves I and III show that increasing the gain of outer compensator F_v can improve dynamic performance; however, phase margins are reduced. Curves I, II, and III demonstrate that I in Eq. (24) is the best.

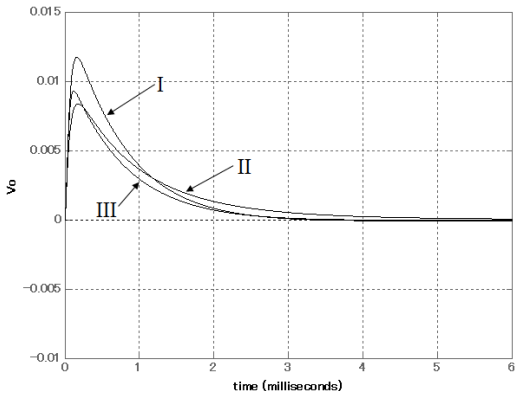

(a) Step response of $\hat{v}_o$ to a step change in $\hat{v}_g$.

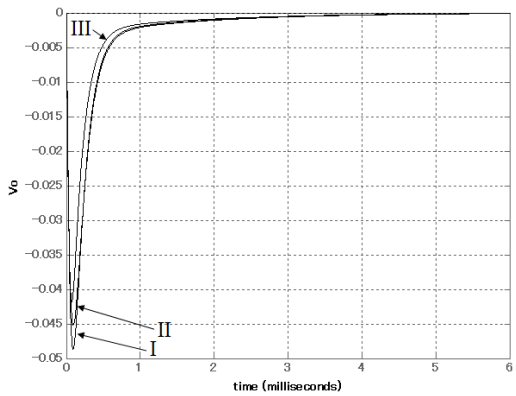

(b) Step response of $\hat{v}_o$ to a step change in $\hat{i}_o$

Fig. 11. Step responses of $\hat{v}_o$.

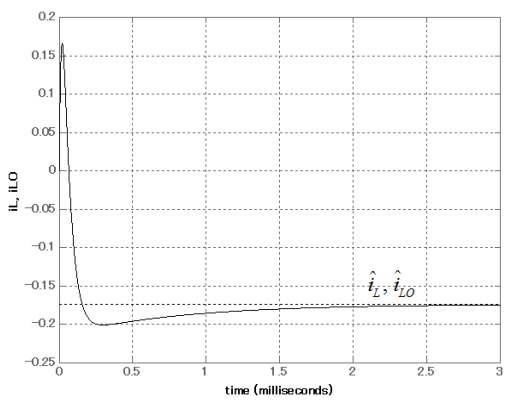

(a) Step responses of $\hat{i}_L$ and $\hat{i}_{LO}$ to a step change in $\hat{v}_g$.

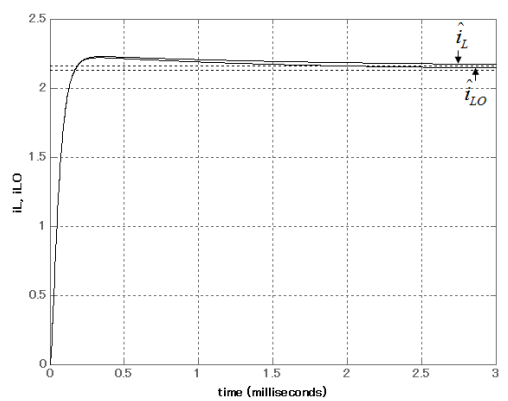

(b) Step response of $\hat{i}_L$ and $\hat{i}_{LO}$ to a step change in $\hat{i}_o$

Fig. 12. Step responses of $\hat{i}_L$ and $\hat{i}_{LO}$.

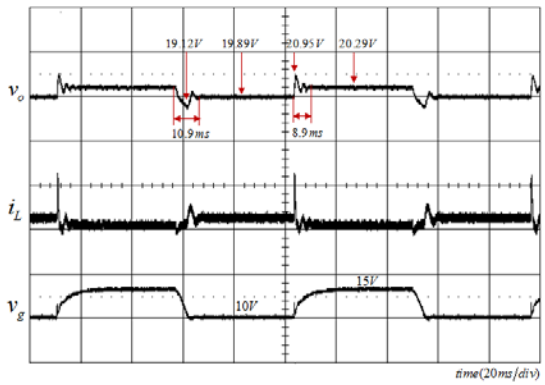

(a) Dynamic response when input voltage is disturbed.

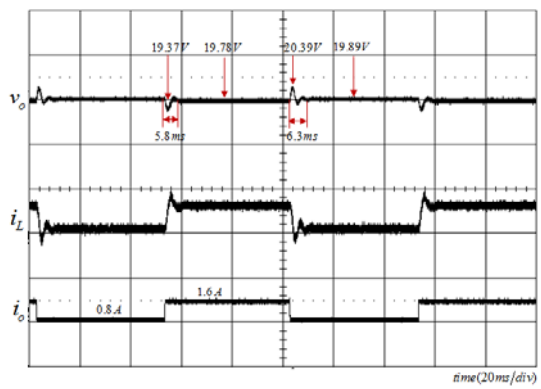

(b) Dynamic response when load current is disturbed.

Fig. 13. Dynamic response of output voltage (H∞ approach).

The closed-loop characteristics of the inductor current $\hat{i}_L$ and estimated inductor current $\hat{i}_{LO}$ can also be easily derived from Fig. 1. For the previously obtained LO and compensator I, the step responses of $\hat{i}_L$ and $\hat{i}_{LO}$ are shown in Fig. 12. The estimated inductor current $\hat{i}_{LO}$ perfectly estimated inductor current $\hat{i}_L$ when the input voltage is disturbed. Meanwhile, a slight error occurs between $\hat{i}_L$ and $\hat{i}_{LO}$ when the load current is disturbed.

C. Practical Experiments of the Sensorless Control of the Boost Converter

The previously presented continuous controller should be discretized to execute the controller on a digital processor. Through bilinear transformation $s = 2(z - 1)/T_s(z + 1)$, where T_s is equivalent to the switching period, the digital counterpart of the controller in Eq. (21) obtained by the proposed H∞ synthesis approach is written in Eq. (26) for w_o = 10 and ε = 1/8,000. The practical dynamic response of output voltage is shown in Fig. 13.

$$\begin{cases} p(k+1) = -9{,}572.3\,p(k) + 53.1831\hat{i}_g(k) - 1{,}242.1v_o(k) \\ \hat{d}(k) = -0.00005\,p(k) - 0.0014\hat{i}_g(k) - 1.0483v_o(k) \end{cases} \quad (26)$$

For LO-based sensorless multi-loop control, the discrete counterpart of Eq. (22) is obtained in Eq. (27) by the zero-hold discretization method. The discrete counterpart of Eq. (23) is obtained in Eq. (28) by the backward difference $s = 1 - z^{-1}/T_s$.

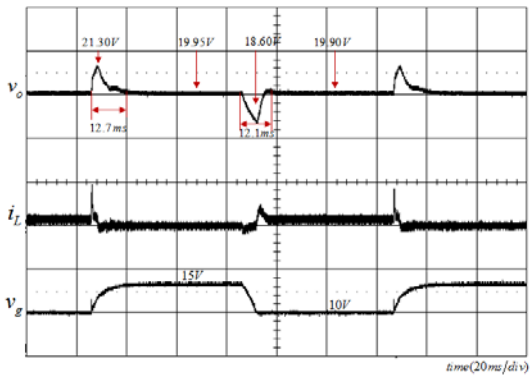

(a) Dynamic response when input voltage is disturbed.

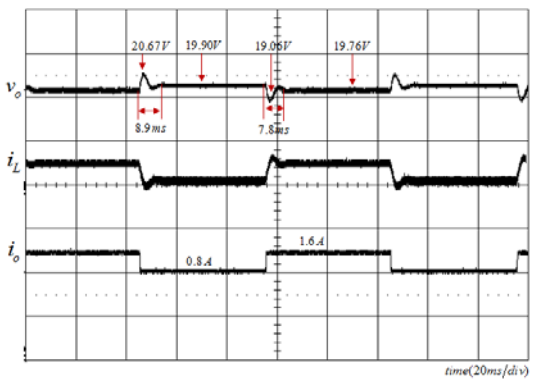

(b) Dynamic response when load current is disturbed.

Fig. 14. Dynamic response of output voltage (LO-based).

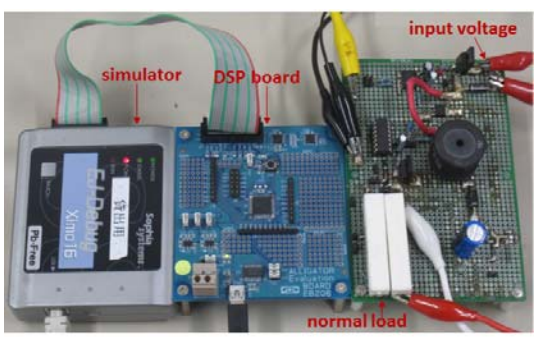

Fig. 15. Experimental environment.

$$\hat{x}(k+1) = A\hat{x}(k) + Bu(k) + L(\hat{v}_o(k) - \hat{v}_{LO}(k)), \quad (27)$$

where $\hat{x}(k) = [\hat{i}_{LO}(k)\ \hat{v}_{LO}(k)]$, $u(k) = [\hat{d}(k)\ \hat{v}_g(k)]$, and

$$A = \begin{bmatrix} 0.9938 & -0.0660 \\ 0.0031 & -0.9996 \end{bmatrix},\ B = \begin{bmatrix} 2.9965 & 0.1414 \\ -0.0067 & 0.0002 \end{bmatrix},$$

$$L = \begin{bmatrix} -0.0988 \\ 4.9993 \end{bmatrix},$$

$$F_m = 0.2 + 0.0017(1 - z^{-1})$$
$$F_v = 30 + 0.1200(1 - z^{-1}) \quad (28)$$

Fig. 14 shows the practical dynamic response by the LO and PI controllers.

Fig. 15 presents the practical experimental environment. A digital 16 bit DSC NJU20010 produced by the NJRC is used to execute the aforementioned digital controllers. The clock frequency of DSC is 62.5 MHz. ADC and PWM are integrated into the DSC. The limit of the duty ratio is set to 0.05–0.88. The slew rates of the load and input voltage are 250 mA/μs and 2.0 V/μs, respectively. A 25 Ω resistor is used as the normal load. An electronic load PLZ164W is used to generate the load current disturbance of 0.8 A. Input voltage is alternated by a switch.

D. Summary

For conventional LO-based sensorless multi-loop controls, six parameters should be determined. An iterative trial-and-error process is needed to determine these parameters. Comparatively, the sensorless controller derived from the proposed H∞ synthesis approach has only one adjustable parameter γ. The closed-loop characteristics evaluation becomes straightforward because this parameter is directly related to the closed-loop characteristics. Figs. 6, 7, and 13 show that better dynamic performance is maintained in the proposed H∞ synthesis approach than in the conventional LO-based sensorless multi-loop control.

VI. Conclusion

For multi-loop control of a boost converter in CCM, closed-loop characteristics and loop gains are generally indirect. The conventional observer-based sensorless multi-loop control severely aggravates the closed-loop characteristics evaluation because more parameters are related to the closed-loop characteristics. The proposed robust H∞ synthesis approach performs a straightforward closed-loop characteristics evaluation by parameterizing the controller with an adjustable parameter. Simulations show the significant advantages of the closed-loop characteristics evaluation, and practical experimental results confirmed the simulation results. The sensorless controller derived by the proposed H∞ synthesis approach is suitable for boost converters. The proposed H∞ synthesis approach is also suitable for the sensorless controller design of other converters, such as buck–boost and quadratic converters.

References

[1] R. Ahmadi, D. Paschedag, and M. Ferdowsi, "Closed-loop input and output impedances of DC-DC switching converters operating in voltage and current mode control," in *36th Annual Conference on IEEE Industrial Electronics Society(IECON)*, pp. 2311-2316, 2010.

[2] H. Choi, "Practical feedback loop design considerations for switched mode power supplies," *Fairchild Semiconductor Power Seminar*, pp. 489-498, 2010-2011.

[3] H. P. Forghani-zadeh and G. A. Rincon-Mora, "Current-sensing techniques for DC-DC converters," in *45th Midwest Symposium on Circuits and Systems*, Vol. 2, pp. 577-580, Aug. 2002.

[4] P. Midya, T. K. Philip, and F. G. Matthew, "Sensorless current mode control—an observer-based technique for DC–DC converters," in *28th Annual IEEE Power*

Electronics Specialists Conference(PESC), Vol. 1, pp. 197-202, Jun. 1997.
[5] G. Cimini, G. Ippoliti, G. Orlando, and M. Pirro, "Current sensorless solution for PFC boost converter operating both in DCM and CCM," in *21st Mediterranean Conference on Control & Automation(MED)*, pp. 137-142, 2013.
[6] A. G. Beccuti, S. Mariethoz, S. Cliquennois, S. Wang, and M. Morari, "Explicit model predictive control of DC–DC switched-mode power supplies with extended kalman filtering," *IEEE Trans. Ind. Electron.*, Vol. 56, No. 6, pp. 1864-18740, Jun. 2009.
[7] D. G. Luenberger, "An introduction to observers," *IEEE Trans. Autom. Control*, Vol. 16, No. 6, pp. 596-602, Dec. 1971.
[8] A. F. Rozman and J. J. Boylan, "Band pass current control," in *Applied Power Electronic Conference and Expression*, Vol. 2, pp. 631-637, Feb. 1994.
[9] R. B. Ridley, B. H. Cho, and F. C. Y. LEE, "An analysis and interpretation of loop gains of multi-loop controlled switching regulators," *IEEE Trans. Power Electron*, Vol. 3, No. 4, pp. 489-498, Oct. 1988.
[10] H. Cho, S. J. Yoo, and S. Kwak, "State observer based sensor less control using Lyapunov's method for boost converters," *IET Power Electron.*, Vol. 8, No. 1, pp. 11-19, Jan. 2015.
[11] R. Naim, G. Weiss, and S. Ben-Yaakov, "H∞ control applied to boost power converters," *IEEE Trans. Power Electron.*, Vol. 12, No. 4, pp. 677-683, Jul. 1997.
[12] E. Vidal-Idiarte, L. Martinez-Salamero, H. Valderrama-Blavi, F. Guinjoan, and J. Maixe, "Analysis and design of H∞ control of nonminimum phase-switching converters," *IEEE Trans. Circuits Syst. I, Fundam. Theory Appl.*, Vol. 50, No. 10, pp. 1316- 1323, Oct. 2003.
[13] C. Olalla, R. Leyva, A. E. Aroudi, P. Garces, and I. Queinnec, "LMI robust control design for boost PWM converters," *IET Power Electron.*, Vol. 3, No.1, pp. 75-85, Jan. 2010.
[14] A. Moran and M. Hayase, "Design of reduced order H∞ controllers," in *Proc. the 36th International Session Papers(SICE) Annual Conference*, pp. 1013-1018, 1997.
[15] C. F. Yung, "Reduced-order H∞ controller design: an algebraic riccati euqation approach," *Automatica*, Vol. 36, No. 6, pp. 923-926, Jun. 2000.
[16] J. Yu and A. Sideris, "H∞ control synthesis via reduced order LMIs," in *36th Conference on Decision & Control*, Vol. 1, pp. 183- 188, Dec. 1997.
[17] P. Gahinet, "Explicit controller formulas for LMI-based H∞ synthesis," *Automatica*, Vol. 32, No. 7, pp. 1007-1014, Jul. 1994.
[18] M. C. Berg, "Introduction to a special coordinate basis for multivariable linear systems," *IEE Proceedings – Control Theory and Applications*, Vol. 145, No. 2, pp. 204-210, Mar. 1998.
[19] A. Saberi, B. M. Chen, and Z. L. Lin, "Closed-form solutions to a class of H∞-optimization problems," *International Journal of Control*, Vol. 60, No. 1, pp. 41-70, 1994.
[20] A. A. Stoorvogel, A. Saberi, and B. M. Chen, "A reduced order observer based controller design for H∞-optimization," *IEEE Trans. Autom. Control*, Vol. 39, No. 2, pp. 355-360, Feb. 1994.
[21] B. M. Chen, *Robust and H∞ control*, Springer, 2010.
[22] B. M. Chen, A. Saberi, and U. L. LY, "A non-iterative method for computing the infimum in H∞-optimization," *International Journal of Control*, Vol. 56, No. 6, pp. 1399-1418, Feb. 1992.
[23] C. Scherer, "H∞-control by state-feedback and fast algorithms for the computation of optimal H∞-norms," *IEEE Trans. Autom. Contr.*, Vol. 35, No. 10, pp. 1090-1099, Oct. 1990.
[24] K. K. Marian, *Pulse-width modulated DC–DC power converters*, John Wiley & Sons, New Jersey, 2008.

Xutao Li received his B.S. degree in Automation from Wuhan Technology University, China in 1999 and M.S. degree in Precise Instrument and Machinery from Shanghai Jiaotong University, China in 2006. He worked for several years in Japan. He received his Ph.D. degree in the Graduate School of Information, Production and Systems, Waseda University, Japan in 2016. His research interests include switching mode power suppliers and control theory.

Minjie Chen received his B.S. degree on Electrical Engineering and Automation from Shanghai Jiaotong University, China in 2009 and M.S. degree from the Graduate School of Information, Production and Systems, Waseda University, Japan. He is currently a Ph.D. candidate in the same school. His research interest includes power converter technology.

Hirofumi Shinohara received his B.S. and M.S. degrees in Electrical Engineering and Ph.D. degree in Informatics from Kyoto University in 1976, 1978, and 2008, respectively. He has engaged in the administration of collaborative studies on VLSI circuits between industry and academy in the Semiconductor Technology Academic Research Center. He is currently a professor at the Graduate School of Information, Production and Systems, Waseda University, Japan. His research interests include advanced SRAM, low-power circuits, and variation aware design.

Tsutomu Yoshihara received his B.S. and M.S. degrees in Physics and Ph.D. degree in Electronic Engineering from Osaka University, Osaka, Japan in 1969, 1971, and 1983, respectively. In 1971, he joined the ULSI laboratory of Mitsubishi Electric Corporation, Hyogo, Japan, where he has been engaged in the research and development of MOS LSI memories. Since April 2003, he has been a professor at the Graduate School of Information, Production and Systems, Waseda University, Japan and is currently involved in research on system LSI. He is a member of the IEEE Solid-State Circuits, IEICE of Japan, and Institute of Electrical Engineers of Japan.